11th International Symposium on Magnetic Bearings
August 26-29, Nara, Japan

INDEPENDENT CONTROL OF TORQUE AND RADIAL FORCE IN BEARINGLESS SWITCHED RELUCTANCE MOTORS

Cao Xin
Nanjing University of Aeronautics and Astronautics, Nanjing, 210016, China,
cxxc118@nuaa.edu.cn

Deng Zhiquan
Nanjing University of Aeronautics and Astronautics, Nanjing, 210016, China,
dzq@nuaa.edu.cn

Yang Gang
Nanjing University of Aeronautics and Astronautics, Nanjing, 210016, China,
sdzbyg@yahoo.com.cn

Wang Xiaolin
Nanjing University of Aeronautics and Astronautics, Nanjing, 210016, China,
wangxl@nuaa.edu.cn

ABSTRACT
Radial force and torque are the control objectives which determine the machine performance of levitation and rotation in a bearingless switched reluctance motor (BSRM). This paper proposes a control scheme for rotating and levitating a 12/8 BSRM. The motor torque and radial force are independently controlled with hybrid excitations in main windings and levitation windings. Firstly, the mathematical relationship between radial force and currents, which is utilized in this work, is derived with Maxwell stress tensor method. Then the proposed control scheme is analyzed. The average torque of each phase generated in levitation region equals to zero for its symmetry of the aligned position. Accordingly, the current calculating algorithm is deduced to minimize the magnitude of instantaneous torque in levitation region. The principle and realization of the proposed scheme are demonstrated with FE analysis. Experimental results show that the proposed scheme is effective for a stable levitation.
Index Terms—bearingless motor, switched reluctance motor, radial force, torque, independent control.

I. INTRODUCTION

Switched reluctance motors(SRM) have been already applied in some special fields for its doubly salient configuration. Its particular characteristics are the simple constructions, low manufacturing cost, fault tolerance, and the ability to operate in a high temperature environment. Due to its doubly salient structure, SRM produces an attractive magnetic force between stator and rotor poles. The force can be divided into tangential and radial components. The tangential force component compels the rotor to rotate, and the radial force component brings along the problem of noise and vibration.

Recently, electric machines usually work at a high speed for a high power density. But a higher rotational speed shortens the mechanical bearing life. This limits the high speed ability of switched reluctance motors. A bearingless technology is developed to avoid the contact and lubrication between motor shaft and bearing. Many researchers have been devoted to integrating the bearingless technology with switched reluctance motors [1]-[12]. The bearingless switched reluctance motors are divided into one set of windings and two sets of windings according to the number of coil windings embedded on the stator. The two kinds of motors generate radial forces both by changing the flux density in the motor air gap. The unbalanced magnetic forces are produced because of the different flux density in the two sides of the rotor. Then the controlled radial forces can pull the shaft back to the geometric center by controlling different flux densities.

In bearingless switched reluctance motors with only one set of winding in each stator pole, two types with different pole pair numbers 12/8 and 8/6 are studied. All pole currents are controlled independently [5]-[12]. In 8/6 BSRM, three windings are loaded with different currents in each commutation period and sum of three torques and three lateral forces supply desired torque and suspending forces [8], [9]. In 12/8 BSRM, a scheme uses

single-phase and two-phase sinusoidal excitation to control radial force and torque [5], [7], [11]. Another scheme controls the torque with the conventional method which all energizing phase currents are the same to produce the desired torque [6], [10]. And two additional poles in the phase with descending-inductance are excited to produce the requested radial force acting on the shaft.

In bearingless switched reluctance motors with two sets of windings, there are a main winding and an auxiliary winding which is called radial force winding on each stator pole [1]-[4]. The main winding is utilized to control the motor torque and produces a bias magnetic field for the radial force generation. The auxiliary winding generates the required radial force for the levitation and also generates an additional motor torque. The mathematical model about the relationship between radial force and motor currents is derived to implement the levitation in practice [1], [2]. In this model, radial force is determined by the main winding and radial force winding currents which vary gradually on different rotor angular position. The control scheme is also discussed and verified experimentally [3], [4]. In this scheme, the commutation period of each phase is fixed but the firing angle can be shifted back and forth to change the commutation position. Therefore the currents and firing angle determine the values of radial force and motor torque together. Another control scheme based on the currents distribution strategy presented in [3] is reported in [12]. In this scheme, the required main winding and auxiliary winding currents are summed and go into a single motor coil per pole. However, the current and firing angle calculating processes in these mentioned schemes is sophisticated and variables are influenced by both of the desired radial force and torque. A more memory resource in digital signal processor is needed to store a look-up table for a good performance. The coupling control of radial force and torque also reduces the motor performance more or less.

In this paper, a novel scheme with hybrid excitations is proposed based on 12/8 bearingless switched reluctance motors with two sets of windings on the stator pole. The scheme uses hybrid excitations in the main winding and single-phase excitation in the radial force winding. The radial force and average torque are controlled independently. The principle and advantage of the scheme is illustrated. And the levitation currents calculation is also derived. The proposed scheme is verified with FE analysis and experiments.

II. TORQUE AND RADIAL FORCE MODEL

Fig.1 shows only phase A stator differential windings configuration of the 12/8 bearingless switched reluctance motor. The arc of the rotor and stator teeth is 15 mechanical degrees (°M). The aligned position is defined as θ=0°. When the two differential windings conduct the currents as shown in Fig.1, the flux density in air gap 1 increased whereas that decreased in air gap 3. So an unbalanced magnetic force is generated toward the positive direction in the α axis. The radial force in the β axis can be also produced in the same way. Then the radial force in any desired direction can be produced by composing the two radial forces in perpendicular directions. The radial force produced by phase B or C can be derived similarly.

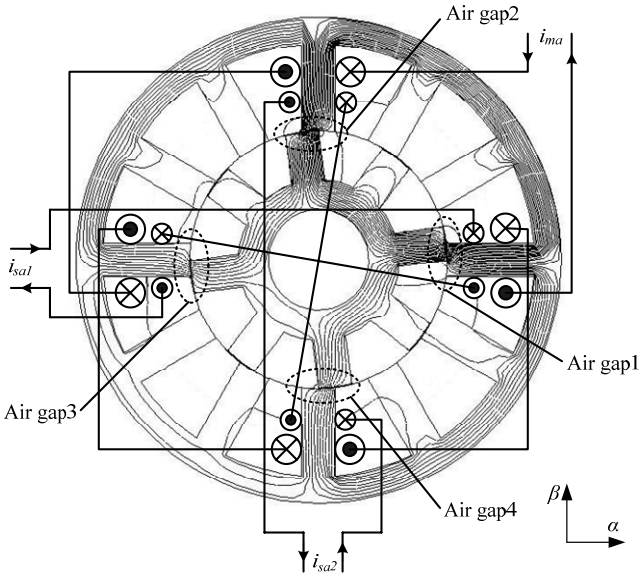

Fig.1 Configuration and flux-line of phase A

A. Maxwell Stress Tensor Method

With the magnetic saturation neglected, the derivation of mathematical model is based on the Maxwell Stress Tensor in this work. Recall the Maxwell Stress Tensor as given in (1), (2), where the resultant force is independent of the integration path[13].

$$F_n = \frac{1}{2\mu_0}\iint_S \left(B_n^{\,2} - B_t^{\,2}\right) dA \tag{1}$$

$$F_t = \frac{1}{\mu_0}\iint_S B_n B_t dA \tag{2}$$

As shown in Fig.2, the relative position of two poles is simplistic to simplify the derivation. The flux paths are supposed to be radial across the air gap, and the flux lines are either orthogonal or parallel to the integration paths. Under these assumptions, the Maxwell stress equation can be simplified as follows:

The integration path is perpendicular to the flux lines:

$$F_n = \frac{1}{2\mu_0}\iint_S B_n^{\,2} dA \tag{3}$$

The integration path is parallel to the flux lines:

$$F_n = -\frac{1}{2\mu_0}\iint_S B_t^2 dA \tag{4}$$

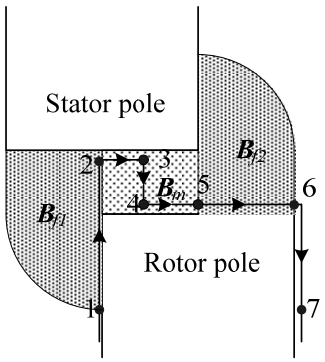

Fig.2 The integration paths with Maxwell stress tensor method

Forces acting on the rotor pole in Fig.2 can be derived by using the above mentioned equations.

The radial force component equals:

$$\begin{aligned} F_r &= \frac{h}{2\mu_0}\left(\int_2^3 B_m{}^2 dl + \int_4^5 B_m{}^2 dl + \int_5^6 B_{f2}{}^2 dl\right) \\ &= \frac{h}{2\mu_0}\left(B_m{}^2\left(l_{23}+l_{45}\right) + B_{f2}{}^2 l_{56}\right) \end{aligned} \tag{5}$$

The tangential force component equals:

$$F_t = \frac{h}{2\mu_0}\left(\int_1^2 B_{f1}{}^2 dl - \int_3^4 B_m{}^2 dl\right) \tag{6}$$

Thus, the torque acting on the rotor pole in Fig.2 can be written as,

$$T = F_t \cdot r = \frac{hr}{2\mu_0}\left(B_{f1}{}^2 l_{12} - B_m{}^2 l_{34}\right) \tag{7}$$

B. Flux Density Calculation

In terms of the straight flux lines, the main flux density can be written as,

$$B_{ma1} = \frac{\mu_0\left(N_m i_{ma} + N_b i_{sa1}\right)}{l_0} \tag{8}$$

The fringing flux density can be also obtained with the straight and circular flux lines as,

$$B_{fa1} == \frac{\mu_0\left(N_m i_{ma} + N_b i_{sa1}\right)}{l_0 + \pi r|\theta|/4} \tag{9}$$

C. Radial Force and Instantaneous Torque Equations

The radial forces produced by phase A in α and β axis can be expressed, respectively, as

$$\begin{aligned} F_\alpha &= F_{a1} - F_{a3} \\ &= \frac{h}{2\mu_0}\left(\begin{array}{l}\left(B_{ma1}{}^2 - B_{ma3}{}^2\right)\left(\frac{\pi r}{12} - r|\theta|\right) \\ +\left(B_{fa1}{}^2 - B_{fa3}{}^2\right) r|\theta|\end{array}\right) \end{aligned} \tag{10}$$

$$\begin{aligned} F_\beta &= F_{a2} - F_{a4} \\ &= \frac{h}{2\mu_0}\left(\begin{array}{l}\left(B_{ma2}{}^2 - B_{ma4}{}^2\right)\left(\frac{\pi r}{12} - r|\theta|\right) \\ +\left(B_{fa2}{}^2 - B_{fa4}{}^2\right) r|\theta|\end{array}\right) \end{aligned} \tag{11}$$

When the magnetic field is linear, the radial forces can be simplified as,

$$F_\alpha = K_f(\theta) i_{ma} i_{sa1} \tag{12}$$

$$F_\beta = K_f(\theta) i_{ma} i_{sa2} \tag{13}$$

Where,

$$K_f(\theta) = \mu_0 hr N_m N_b \left(\begin{array}{l}\frac{\left(\pi - 12|\theta|\right)}{6l_0{}^2} \\ +\frac{32|\theta|}{\left(4l_0 + \pi r|\theta|\right)^2}\end{array}\right) \tag{14}$$

The net torque by phase A is

$$\begin{aligned} T_a &= T_{a1} + T_{a2} + T_{a3} + T_{a4} \\ &= J_t(\theta)\left(2N_m{}^2 i_{ma}{}^2 + N_b{}^2 i_{sa1}{}^2 + N_b{}^2 i_{sa2}{}^2\right) \end{aligned} \tag{15}$$

When generating a positive torque,

$$J_{tp}(\theta)\big|_{\theta\le 0} = \mu_0 hr\left(\frac{1}{l_0} - \frac{16\left(l_0 - r\theta\right)}{\left(4l_0 - \pi r\theta\right)^2}\right) \tag{16}$$

On the contrary, the coefficient $J_t(\theta)$ at the negative torque region is

$$J_{tn}(\theta)\big|_{\theta\ge 0} = \mu_0 hr\left(-\frac{1}{l_0} + \frac{16\left(l_0 + r\theta\right)}{\left(4l_0 + \pi r\theta\right)^2}\right) \tag{17}$$

D. Modification with FE analysis

Due to that the selection of integration paths and some assumptions which could affect the accuracy of the proposed model are utilized in the deriving process, it is necessary to take a modification to eliminate these negative influences. In view of the radial forces

generated region with the proposed control scheme, the modification focus on the angle position from -7.5° to 7.5°. Figure 3 shows the radial forces calculated respectively by the modified model and FE analysis. It is observed that the proposed modified model and FEM results agree well. And therefore, the modified model is used in this paper for its convenience and accuracy in calculating radial forces. The modification relative to $K_f(\theta)$ can be written as,

$$K'_f(\theta) = K_f(\theta)\left(1 + k_1|\theta| + k_2|\theta|^2 + k_3|\theta|^3\right) \quad (18)$$

Where, k_1=0.8, k_2=-4, k_3=12.

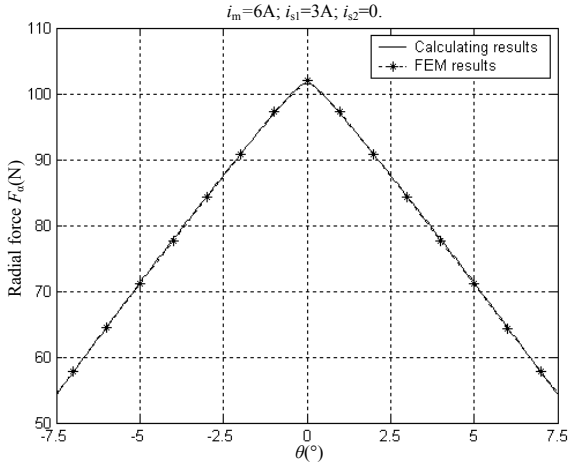

Fig.3 FEM results and calculating results

III. PRINCIPLE OF NEW CONTROL SCHEME

A. Proposed Independent Control Scheme

The conduction width of main winding and radial force winding currents was fixed at 15°M in [3]. And advanced angle θ_m was introduced to change positive-torque region. Given that θ_m equaled to zero and radial forces were also constant, the average torque will become zero because of the symmetry of phase inductance. Under such condition, the currents conduction period including main winding currents and levitation currents is from -7.5°M to 7.5°M. Then the additional average torque generated by levitation currents is zero. For a required total average torque, the firing angle of main winding currents can be advanced while that of levitation currents keeps constant. The schematic diagram of phase A is shown in Fig. 4 to illustrate the principle of the proposed control scheme.

Mode I ($\theta \in [\theta_{on}, -\pi/24]$): In this mode, phase A is in the ascending-inductance region. Its main winding is excited to generate positive torque, while levitation current is zero so that phase A does not produce any radial forces. The needed radial force is generated by phase C which produces negative torque in the descending-inductance region. Thus it is two-phase excitation in this mode. The motor's instantaneous torque is the sum of torques produced by phase A and C,

$$T_1 = J_{tp}(\theta)\cdot\left(2N_m{}^2 i_{ma1}{}^2\right) + J_{tn}(\theta+\frac{\pi}{12})\cdot\left(2N_m{}^2 i_{mc2}{}^2 + N_b{}^2 i_{sc1}{}^2 + N_b{}^2 i_{sc2}{}^2\right) \quad (19)$$

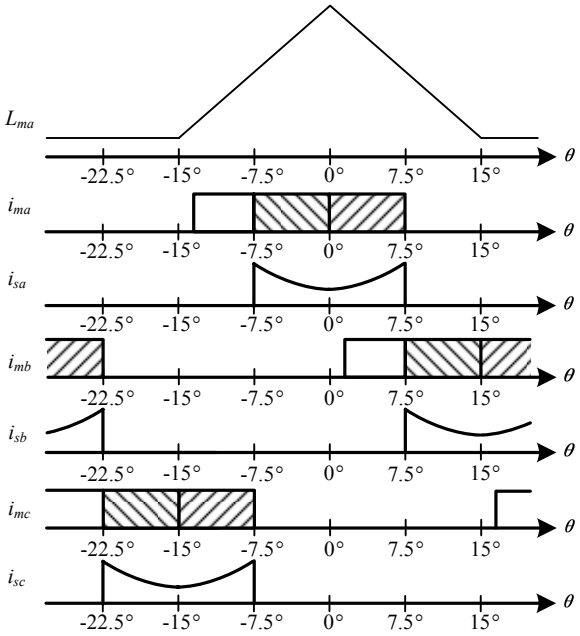

Fig.4 Idealized current waveforms with proposed control scheme

Mode II ($\theta \in (-\pi/24, 0)$): Phase A is still in the ascending-inductance region and generates a positive torque. Radial force is generated by phase A instead of phase C. It is one-phase excitation in this mode and the instantaneous torque is simple as,

$$T_2 = J_{tp}(\theta)\cdot\left(2N_m{}^2 i_{ma2}{}^2 + N_b{}^2 i_{sa1}{}^2 + N_b{}^2 i_{sa2}{}^2\right) \quad (20)$$

Mode III ($\theta \in [0, \pi/12+\theta_{on}]$): In this mode, phase A is in the descending-inductance region and still produced the desired radial force. It creates negative torque and the main winding of phase B is energized to produce positive torque in its own Mode I. The instantaneous torque is expressed as,

$$T_3 = J_{tn}(\theta)\cdot\left(2N_m{}^2 i_{ma2}{}^2 + N_b{}^2 i_{sa1}{}^2 + N_b{}^2 i_{sa2}{}^2\right) \quad (21)$$

Mode IV ($\theta \in (\pi/12+\theta_{on}, \pi/24]$): Phase A still supplies the required radial force, and the main winding currents of phase B begin to fire for the positive torque in its ascending-inductance region. It is two-phase excitation and the instantaneous torque can be written as,

$$T_4 = J_{tp}(\theta - \frac{\pi}{12}) \cdot \left(2N_m{}^2 i_{mb1}{}^2\right) + J_{tn}(\theta) \cdot \left(2N_m{}^2 i_{ma2}{}^2 + N_b{}^2 i_{sa1}{}^2 + N_b{}^2 i_{sa2}{}^2\right) \quad (22)$$

The operation modes of phase B and C can be also derived in the same way. From the above illustration, it can be seen that BSRM is excited by hybrid excitations which composes one-phase excitation with two-phase excitation in main windings, whereas only one-phase excitation in radial force windings. The average torque generated by levitation currents is zero to avoid the problem of additional torques in conventional scheme.

B. Average torque Calculation

Due to the average torque generated in mode II, III, and IV relative to each phase equals to zero, the total average torque can be derived from the integral of the instantaneous torque in mode I of phase A as

$$T_{avg} = \frac{3}{\pi/4}\int_{\theta_{on}}^{-\pi/24} J_{tp}(\theta) \cdot 2N_m{}^2 i_{m1}{}^2 d\theta = G_{tm}{}'(\theta_{on}) i_{m1}{}^2 \quad (23)$$

Where, $-\pi/12 \le \theta_{on} \le -\pi/24$.

$$G_{tm}{}'(\theta_{on}) = \frac{24}{\pi} N_m{}^2 \mu_0 hr \left\{ -\frac{\pi + 24\theta_{on}}{24 l_0} + 2 \times \left[\frac{1}{\pi r} \ln\left(\frac{\pi^3 r^2 + 24\pi(\pi+2) r l_0 + 1152 l_0{}^2}{576\left[\pi r^2 \theta_{on}{}^2 - (\pi+2) r \theta_{on} l_0 + 2 l_0{}^2\right]} \right) + \frac{2}{\pi(\pi-2) r} \ln\left(\frac{\left(\pi^2 r^2 + 24\pi r l_0\right)\left(2\pi r^2 \theta_{on} - 4 r l_0\right)}{\left(\pi^2 r^2 + 48 r l_0\right)\left(2\pi r^2 \theta_{on} - 2\pi r l_0\right)} \right) \right] \right\} \quad (24)$$

Due to that the radial force winding is excited by one-phase excitation, the instantaneous radial forces of phase A can be expressed as,

$$\begin{bmatrix} F_\alpha \\ F_\beta \end{bmatrix} = i_{ma2} \begin{bmatrix} K'_f(\theta) & 0 \\ 0 & K'_f(\theta) \end{bmatrix} \begin{bmatrix} i_{sa1} \\ i_{sa2} \end{bmatrix} \quad (25)$$

From the mentioned analysis, it is shown that the total average torque is determined by i_{m1} and θ_{on}, while the instantaneous radial force is related to i_{m2} and i_s. So the average torque and radial force can be controlled by different variables, and the objective of independent control is achieved.

C. FEM Analysis of Proposed Control Scheme

The maximum average torque decreased in the proposed control scheme because of the currents conducted in the negative-torque region. To obtain a larger average torque, we can advance the turn-on angle of main winding currents as many as possible. Then the average torque can be adjusted by changing i_{m1} and the radial forces are controlled like previous analysis.

Let the main winding and radial force winding conduct from -22.5°M and 0°M, where i_m=6A, i_{s1}=i_{s2}=3A. The waveforms of generated torque and radial force with FE analysis are shown in Fig.5. FEM results suggest that the radial force generated between -22.5°M and -15°M is so small that it can be neglected, meanwhile, the electromagnetic torque increases gradually. It also can be seen that the produced radial force increases and the torque decreases as rotor moves to 0°M. Therefore, the proposed scheme makes a compromise in order to produce average torque and radial forces as large as possible.

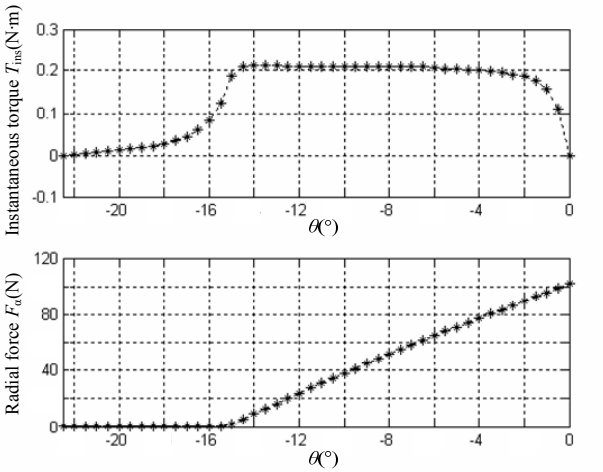

Fig.5 Radial force and instantaneous torque from -22.5 °M to 0 °M with FEM

IV. Levitation Currents Calculation

In the proposed control scheme, the sum of the torque generated by the levitation currents i_{m2} and i_s equals to zero. So the magnitude of instantaneous torque produced in levitation region should be reduced as many as possible to improve the driving efficiency. Given that magnitude of a vector composed of the instantaneous radial forces F_α and F_β can be written as,

$$F^2 = F_\alpha{}^2 + F_\beta{}^2 \quad (26)$$

The F and T can be expressed as,

$$\begin{cases} F = K'_f(\theta) i_{m2} \sqrt{i_{s1}{}^2 + i_{s2}{}^2} \\ T = J_t(\theta)\left[2N_m{}^2 i_{m2}{}^2 + N_b{}^2\left(i_{s1}{}^2 + i_{s2}{}^2\right)\right] \end{cases} \quad (27)$$

Then an inequation relative to T can be derived as,

$$|T| \geq 2\sqrt{2}\left|J_t(\theta)\right| N_m N_b i_{m2} \sqrt{{i_{s1}}^2 + {i_{s2}}^2} \tag{28}$$

When $|T|$ gets a minimum,

$$2{N_m}^2 {i_{m2}}^2 = {N_b}^2 \left({i_{s1}}^2 + {i_{s2}}^2\right) \tag{29}$$

The current i_{m2} can be derived from (28) and (30) as,

$${i_{m2}}^2 = \frac{N_b F}{\sqrt{2} N_m K_f^{'}(\theta)} \tag{30}$$

Where, $-\pi/24 \leq \theta \leq \pi/24$.

Fig.6 shows the calculating process of currents commands between -7.5°M and 7.5°M. It is seen that radial forces F_α^* and F_β^* compose F. Then F and rotating angle θ are submitted into (30) to calculate ${i_{m2}}^*$. In experiments, the coefficient related with θ is precalculated and stored as a look-up table in the controller in order to reduce the sampling time of a digital signal processor.

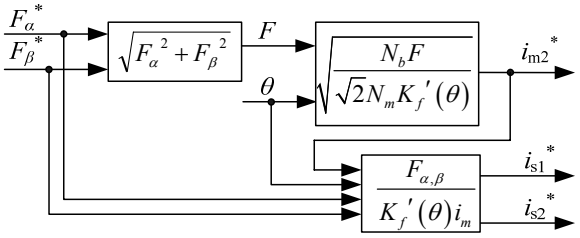

Fig.6 Currents calculating algorithm in levitation region

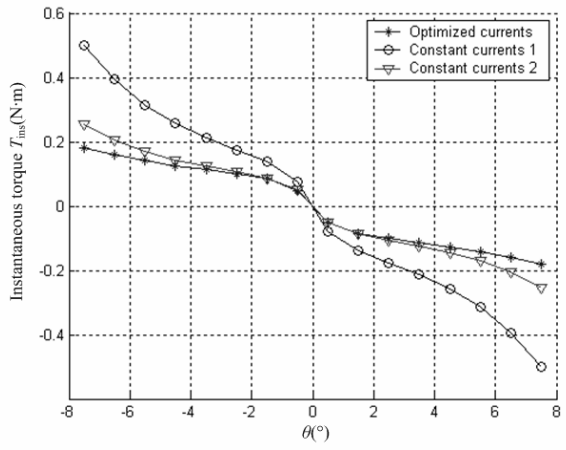

Fig.7 Comparison of torques with optimized currents and constant currents

Fig.7 shows a set of instantaneous torques produced by different currents which generates approximately equal radial forces in FEM. It is seen that the optimized current i_{m2} generates the minimum torque, which verifies the above analysis.

The torque and radial forces produced by phase A can be seen in Fig.8. The given radial force in the α axis is 60N whereas 30N in the β axis. The currents are precalculated with the algorithm as shown in Fig.7. It shows that the torque is odd symmetry about zero point in [-7.5°, 7.5°] and radial forces are near zero in [-22.5°, -7.5°]. So the average torque in [-7.5°, 7.5°] is zero and the generated radial forces can be neglected in [-22.5°, -7.5°].

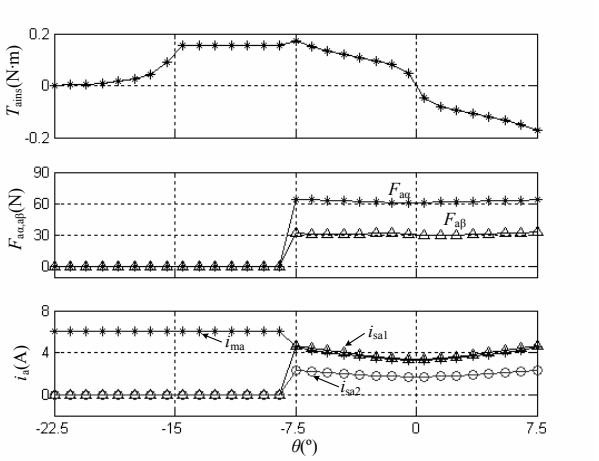

Fig.8 FEM results of radial forces and torque produced by phase A with proposed scheme

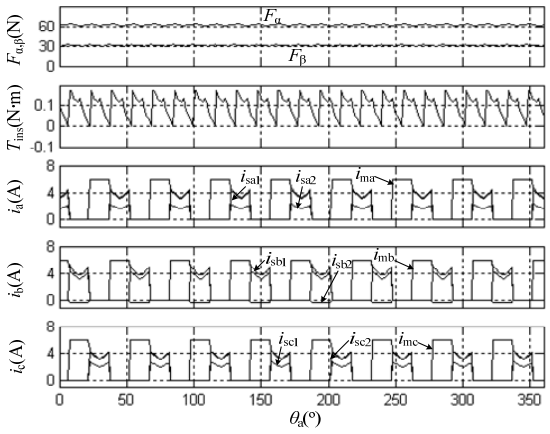

Fig.9 FEM results of radial forces and torque waveforms with proposed scheme from 0 °M to 360 °M

The calculated currents and FE results including radial forces and torque with the proposed independent control scheme are shown in Fig.9. θ_a is rotor angle of phase A defined as θ_a=0 at an aligned position. Note that the currents near the aligned position are smaller than that in the other position for the same radial force. The radial forces and average torque generated with conventional scheme are shown in Fig.10 where the turn-on angle is -9° and the turn-off angle is 6°. The magnitudes of radial forces and average torque generated with the two

different schemes as shown in Fig.9 and Fig.10 are approximately same. It is seen that the peak to peak amplitude of generated torque with proposed scheme is reduced by hybrid excitations. So we can obtain a smoother torque by utilizing reasonable currents. Similarly, motor's vibration and noise can also be controlled actively by certain current distribution[14]. These researches beyond the scope of this paper and will be expounded in future works.

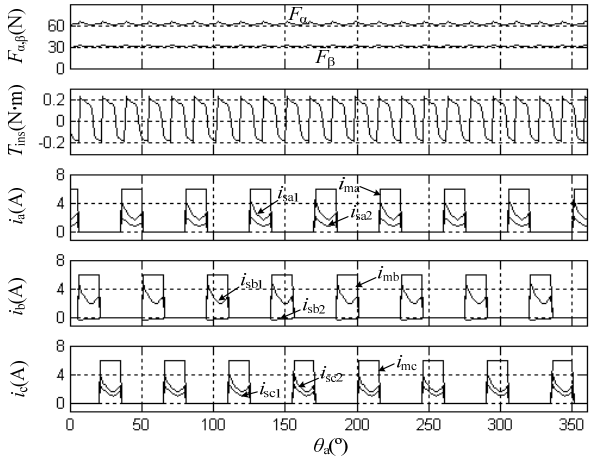

Fig.10 FEM results of radial forces and torque waveforms with conventional scheme from 0 ° to 360 °

V. CONTROL SYSTEM

Fig.11 illustrates how the motor's levitation and rotation are achieved simultaneously with proposed control scheme. The motor speed is regulated with a PI controller, and the output is then converted to the current command as the active phase i_{m1}^*. The rotor radial displacements at the two perpendicular directions are measured and then regulated with PID controller, and the outputs are desired radial forces F_α^* and F_β^*. The two desired radial forces and rotor's rotating angle are inputted to the levitation algorithm whose output are levitation current command i_s^* and main winding current command i_{m2}^*. These current commands are all calculated in a digital signal processor and tracked by inverters in main winding and radial force winding in order to rotate and levitate the rotor.

VI. EXPERIMENTAL RESULTS

The proposed control scheme was verified experimentally. The dimensions of the test motor are shown in Table I. The motor is placed horizontally to apply the rotor's weight as an external force in the β axis.

Fig.12 shows the current and rotor's displacement waveforms with proposed control scheme. The turn-on angle is -18.75°. It is seen that the currents in levitation region such as i_{m2} and i_s are not influenced by a variation of speed.

Fig.13 shows the waveforms of main winding current i_m, radial force winding current i_s, rotational speed, and rotor radial displacements α and β with the speed accelerating from 2000 r/min to 3000 r/min. It is seen that the test motor operates stably under the acceleration except a small perturbation at the beginning in the β axis.

TABLE I: Dimensions of the test motor

Number of turns of motor main	14 turns
Number of turns of motor radial force	17 turns
Arc angle of rotor and stator teeth	15 degree
Outside diameter of stator core	120 mm
Inside diameter of stator pole	60.5 mm
Average air-gap length, l_0	0.25 mm
Inner diameter of rotor	30 mm
Radius of rotor pole, r	30 mm
Stack length, h	75 mm

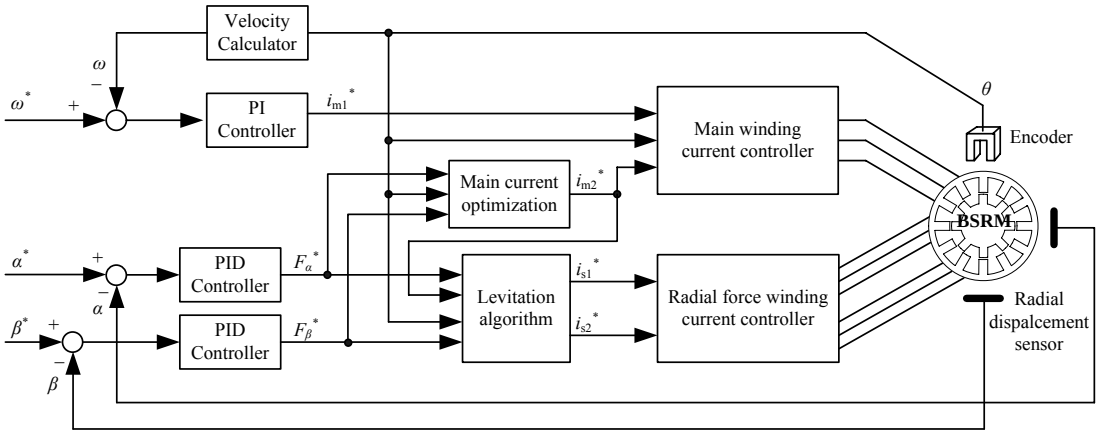

Fig.11 Experimental control block

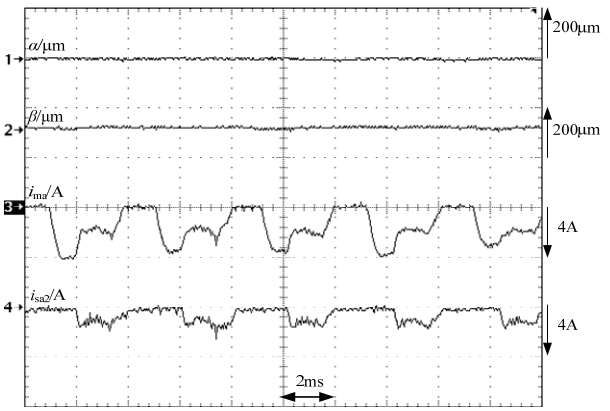

Fig.12 Radial displacements and currents waveforms with the proposed scheme at a speed of 2000 r/min.

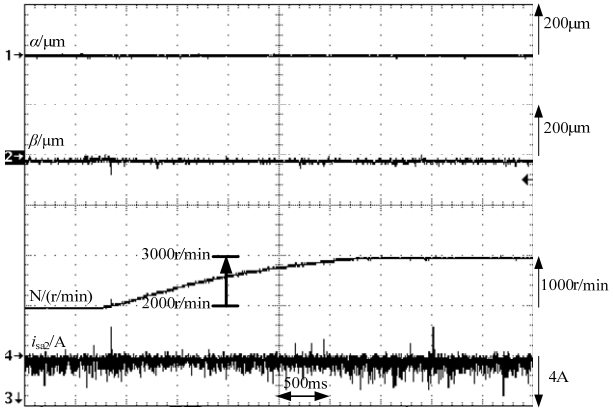

Fig.13 Acceleration with the proposed scheme

VII. CONCLUSION

In the paper, an independent control scheme of bearingless switched reluctance motors is analyzed. The radial force and torque can be separately controlled by different variables. An expression of radial force is used to calculate currents in levitation region, whereas motor average torque control does not need any mathematical model but only a PI controller, which simplifies control algorithm.

The proposed scheme does not need a more memory resource to store a large look-up table. It is suitable for industrial application. Moreover, the radial force is generated around the aligned position where the force can be effectively produced. Also, it is better that the controls of radial force and torque are not coupled. A disadvantage is that a negative torque is produced because the descending-inductance region is used for levitation. Thus some remedial measures are discussed to solve this problem and verified to be effective with FE analysis and experiments.

References

[1] M. Takemoto, K. Shimada, A. Chiba, and T. Fukao, "A design and characteristics of switched reluctance type bearingless motors," in Proc. 4th Int. Symp. Magnetic Suspension Technology, May 1998, pp. 49-63.

[2] M. Takemoto, H. Suzuki, A. Chiba, T. Fukao, and M. A. Rahman, "Improved analysis of a bearingless switched reluctance motor," IEEE Trans. Ind. Appl., Vol. 37, no. 1, pp. 26-34, Jan./Feb. 2001.

[3] M. Takemoto, A. Chiba, and T. Fukao, "A method of determining the advanced angle of square-wave currents in a bearingless switched reluctance motor," IEEE Trans. Ind. Appl., Vol. 37, no. 6, pp. 1702-1709, Nov./Dec. 2001.

[4] M. Takemoto, A. Chiba, H. Akagi, and T. Fukao, "Radial force and torque of a bearingless switched reluctance motor operating in a region of magnetic saturation," IEEE Trans. Ind. Appl., Vol. 40, no. 1, pp. 103-112, Jan./Feb. 2004.

[5] F. C. Lin and S. M. Yang, "Instantaneous shaft radial force control with sinusoidal excitations for switched reluctance motors," in Proc. IEEE IAS Annu. Meeting, Seattle, WA, Oct. 2004, pp. 424-430.

[6] W. T. Liu and S. M. Yang, "Modeling and control of a self-bearing switched reluctance motor," in Proc. IEEE IAS Annu. Meeting, Kowloon, Hong Kong, Oct. 2005, pp. 2720-2725.

[7] F. C. Lin and S. M. Yang, "Radial force control of a switched reluctance motor with two-phase sinusoidal excitations," in Proc. IEEE IAS Annu. Meeting, Tampa, FL, Oct. 2006, pp. 1171-1177.

[8] L. Chen and W. Hofmann, "Analytically computing winding currents to generate torque and levitation force of a new bearingless reluctance motor," EPE-PEMC 2006., Portoroz Slovenia, Sep./Oct. 2006, pp. 1058-1063.

[9] L. Chen and W. Hofmann, "Performance characteristics of one novel switched reluctance bearingless motor drive," in Power conversion conference 2007., Nagoya, Japan, Apr. 2007, pp. 608-613.

[10] F. C. Lin and S. M. Yang, "An approach to producing controlled radial force in a switched reluctance motor," IEEE Trans. Ind. Electron., Vol. 54, no. 4, pp. 2137-2146, Aug. 2007.

[11] F. C. Lin and S. M. Yang, "Self-bearing control of a switched reluctance motor using sinusoidal currents," IEEE Trans. Power Electron., Vol. 22, no. 6, pp. 2518-2526, Nov. 2007

[12] B. B. Choi and M. Siebert, "A bearingless switched reluctance motor for high specific power applications," in 42nd AIAA/ASME/SAE/ASEE Joint Propulsion Conference & Exhibit, Sacramento, California, Jul. 2006.

[13] N. R. Garrigan, W. L. Soong, C. M. Stephens, A. Storace, and T. A. Lipo, "Radial force characteristics of a switched reluctance machine," in Proc. IEEE IAS Annu. Meeting, 1999, Vol. 4, pp. 2250-2258.

[14] J. W. Ahn, S. J. Park, D. H. Lee, "Hybrid excitation of SRM for reduction of vibration and acoustic noise," IEEE Trans. Ind. Electron., Vol. 51, no. 2, pp. 374-380, Apr. 2004.